RSC Advances

ROYAL SOCIETY OF CHEMISTRY

www.rsc.org/advances

Controllable synthesis of hierarchical mesoporous/microporous nitrogen-rich polymer networks for CO_2 and Cr (VI) ion adsorption

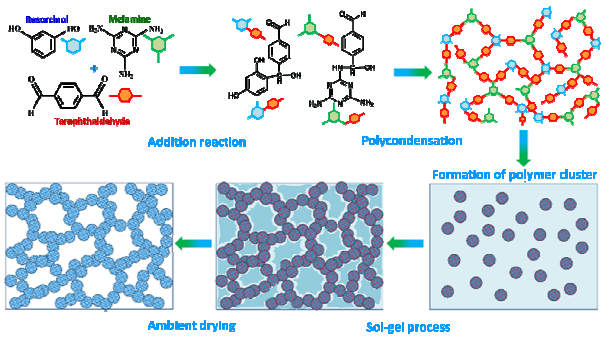

A facile and scalable one-pot approach has been developed for the preparation of hierarchical meso-and microporous nitrogen-rich polymer networks by sol-gel polymerization of melamine, resorcinol and terephthaldehyde.

RSC Advances

RSCPublishing

ARTICLE

Controllable Synthesis of Hierarchical Mesoporous/ Microporous Nitrogen-Rich Polymer Networks for CO_2 and Cr (VI) Ion Adsorption

Cite this: DOI: 10.1039/x0xx00000x

Received 00th January 2012,
Accepted 00th January 2012

DOI: 10.1039/x0xx00000x

www.rsc.org/

Jitong Wang, †,[a] Sheng Xu, †,[a] Yuefeng Wang,[a] Rong Cai,[b] Chunxiang Lv, *,[b] Wenming Qiao,[a] Donghui Long, *,[a] and Licheng Ling[a]

A facile and scalable one-pot approach has been developed for the preparation of hierarchical meso-and microporous nitrogen-rich polymer networks by sol-gel polymerization of melamine, resorcinol and terephthaldehyde. The obtained polymer networks have hierarchical porous structure with moderate microporous surface area and high mesoporous volume. The micropores are within the networks of highly cross-linked polymer chains, while the mesopores result from a 3-D continuous polymeric gel network formed by the reaction-induced sol-gel phase separation. The addition of hexafunctional melamine in the polymer precursor could enhance the crosslinking degree in molecular level, thus creating more accessible micropores within the networks. It can also increase the size of polymer clusters, leading to the formation of larger mesopores. Moreover, the nitrogen functional groups inherited from melamine and the –OH functional groups from resorcinol can also be adjusted by changing the precursor composition. These rich surface functional groups could serve as irregular sites with chemical heterogeneity available for CO_2 and chromium Cr (VI) ion adsorption. High CO_2 uptake up to 2.4 mmol/g and high chromium adsorption capacity of 126.3 mg/g are obtained. The outstanding advantages of the MRT networks present here include their low price, commercially available starting compounds and the easy way of synthesis. This promises this kind of new porous polymers with tailored physical and chemical properties for further applications.

Introduction

Microporous polymer networks are a rapidly expanding class of porous materials constructed from smaller organic building blocks and exhibit large surface areas, small pore sizes and low densities.[1-3] They have attracted considerable scientific attention for their potential opportunities for new science and technological applications in catalysis, [4-6] chemical separations[7] and gas storage [8-10]. Several design strategies have been reported to produce the polymer with permanent microporosity. i) Hypercrosslinked polymers (HCPs) on a multiple Friedel-Crafts alkylation of swollen polystyrene,[11] poly(chloromethylstyrene),[12] polyaniline,[13] and polyfunctional benzyl chlorides,[14] where extensive crosslinking prevents close packing of polymeric chains. ii) Polymers of intrinsic microporosity (PIMs), [15, 16] where polymers are prepared from rigid, contorted structures that inhibit the efficient packing of the polymer chains and therefore result in micropores being formed between polymer layers. iii) Conjugated microporous polymers (CMPs), [17, 18] in which the inherent rigidity of most conjugated π-systems lends well to the generation of permanent microporosity, iv) Covalent organic frameworks (COFs),[19-22] which are crystalline materials formed by reversible condensation of appropriate multifunctional building blocks, v) Organic molecular networks (OMNs), whereby colloidal dispersions (sols) of microporous molecular networks were formed via the crosslinking polymerization of multi-functional monomers, with these sols being sufficiently processable to yield particles and films.[23-25] All these synthetic strategies are to prepare the polymer consist of linking together rigid organic units, in order to impart rigidity within the network and provide directionality for the formation of the extended network. The rigidity prevents collapse of the network upon itself and results in free volume which becomes the pores within a framework. The rich organic synthesis chemistry could provide good flexibility for the material design to achieve desirable pore properties (surface area, pore volume, pore diameter, etc.).[3]

However, forming polymer network with only permanent microporosity is not enough; they will unequivocally suffer from pore blockage in some applications due to the lack of large pores as transport and diffusion pathways. Hierarchically porous structure provides synergies between transport properties and enhanced surface.[26] Integrating permanent microporosity (< 2 nm) with three-dimensional (3D) continuous mesopores (2-50 nm) or macopores (> 50 nm) is of particular significance because it combines high specific surface area with high pore accessibility desired. Such efforts have been successful to some extent, for example, by surfactant mediated polymerization of phlorglucinol and terephthalaldehyde. Kanatzidis et al.[27] reported that the surfactant cetylpyridinium bromide would be self-assembled with phlorglucinol-terephthalaldehyde framework, and then be removed by washing, leading to the formation of mesopores. They further prepared polymeric organic framework aerogels by polymerization of 1,5-dihydroxynaphthalene with terephthalaldehyde.[28] The hierarchical meso-and macropores could be obtained as a result of the aerogel structure by a supercritical drying. However, up to now, the methods for

direct formation of hierarchical mesoporous/microporous polymer blocks are rarely reported. Additional novel strategies for formation of hierarchical porous polymers are thus highly desired, which need appropriate rigidity of the monomer unit and resultant network structure to avoid the collapse of pores during drying. And the process of making them needs to be simple, versatile and controllable.

In addition to the physical structure of the pores, the functionalities of the polymer framework and pore surface chemistry are also important for their applications.[29-31] By having the ability to control the chemical environment within the pores of microporous networks, it is able to tune a network's interactions with guest molecules, making them increasingly tailored for specific applications.[32] Schwab et al.[33] reported a method toward the synthesis of nitrogen-rich polymer networks through Schiff-base condensation of melamine and aldehydes. Significant amounts of nitrogen issued from melamine have been incorporated into the polymer networks, which may be beneficial for the storage of gases or the stabilization of metal species. Cooper et al.[34] incorporated a range of chemical functionalities including carboxylic acids, amines, hydroxyl groups, and methyl groups into conjugated microporous polymer networks. They suggested that the polar acidic functionalities might outperform aromatic amine functionalities for CO_2 sorption. Li et al.[35] fabricated an N-doped porous carbon with magnetic nanoparticles formed in situ through simple impregnation then polymerization and calcination. The basic nitrogen functionalities increase the negative charge density and simultaneously increase the adsorption of metallic cations. Nevertheless, it remains a great challenge to place desired functionalities and to control over their amount within a network for special applications.

Herein, we reported a facile and one-pot method to directly prepare hierarchically porous polymers with controllable porous structure and chemical composition merely by a sol-gel polymerization of melamine, resorcinol and terephthaldehyde. By removal of the solvent retained in the pores, the obtained melamine-resorcinol-terephthaldehyde (MRT) polymer networks simultaneously possessed micro-and mesopores. The micropore was within the networks of highly cross-linked polymer chains, while the mesopore resulted from a 3D continuous polymeric gel network. The porous structure both at micro-and meso- scale could be easily controlled by simple tuning of the ratio of melamine to resorcinol in the precursors. The amine groups from melamine and the hydroxyl groups from resorcinol can be placed in the networks and their amount can be easily controlled over. We further studied the CO_2 adsorption and chromium Cr (VI) ion adsorption properties for these hierarchical MRT networks. High CO_2 uptake up to 2.5 mmol/g and high chromium adsorption capacity of 126.3 mg/g were obtained. Moreover, the outstanding advantages of the MRT networks present here include their low price, commercially available starting compounds and the easy way of synthesis, whereas other synthetic pathways often rely on costly reaction conditions and/or building blocks. This promises this kind of new porous polymers with tailored physical and chemical properties for further applications.

Experimental

Preparation of the MRT networks

All starting materials and solvents were purchased from Titanchem Co. and used without further purification. In a typical synthesis, 20 mmol melamine (M, Molecular weight: 126.12), 20 mmol of resorinol (R, Molecular weight: 30.03) and 40 mmol terephthaldehyde (T, Molecular weight: 134.13) were dissolved in 60 ml dimethyl sulfoxide (DMSO). The mixture was stirred at 60 ^oC for 1h. Then, the mixed solution was transferred into a Teflon-lined autoclave of 90 ml volume and heated at 180 ^oC for 24 h. After that, the autoclave was cooled down to ambient temperature naturally and a polymeric gel was obtained. The DMSO present in the polymeric gel was exchanged with ethanol for several times. Then the gel was dried in an oven at 60 ^oC for 24 h to obtain the MRT networks. In this work, the mole ratio of M to R was changed from 1-4, while their total reactant mole was fixed at 40 mmol and other variables were fixed. The obtained samples were denoted as MRT-x, where x stands for the M/R ratio. It is worthy noted that the initial M/R ratio is very important to form the gel structure. Low M/R ratio (< 0.5) could not form solid products while high M/R (> 5) caused the formation of particulate precipitates.

Characterization

Elemental analysis was carried out using Elemental Vario EL III. The carbon (C), hydrogen (H), and nitrogen (N) contents were determined directly using the thermal conductivity detector.

Fourier transform infrared (FTIR) spectra of samples were collected by a Nicolet 5S×C FTIR system. Each sample was first finely ground and then diluted with KBr to give a KBr/MRF weight ratio of 200. The FTIR spectra were recorded by accumulating 400 scans at a spectra resolution of 1 cm^{-1}.

The solid-state NMR spectra were measured on a Bruker AVANCE 400 spectrometer operating at 100.6 MHz for ^{13}C. The ^{13}C Cross-Polarization with Magic Angle Spinning (CP/MAS) experiments were carried out at MAS rates of 10 kHz using densely packed powders of the PPNs in 4 mm ZrO_2 rotors. The ^{13}C CPMAS measurements carried out at spinning rate 10 kHz. ^{13}C NMR chemical shifts are reported in ppm downfield relative to tetramethylsilane (TMS) as zero ppm, calibrated using adamantane (38.3 ppm) as a secondary standard.

Thermogravimetry analyses (TGA) were performed under N_2 on a TA Q600 Thermogravimetric Analyzer, with a heating rate of 5 ^oC/ min.

The morphologies of samples were observed under scanning electron microscopy (SEM, JEOL JSM-7500F) and transmission electron microscopy (TEM, JEOL 2100F). The samples were grinded before observation.

Nitrogen adsorption/desorption isotherms were measured at 77 K with a Quadrasorb SI analyser. Before the measurements, the samples were degassed in vacuum at 423 K for 12 h. The Brunauer-Emmett-Teller (BET) method was utilized to calculate the specific surface area. Total pore volume was estimated from adsorbed amount at P/P_0 = 0.985. The mesoporous pore size and pore volume were derived from desorption branch by using the Barrett-Joyner-Halenda (BJH) model. The micropore size distribution and micropore surface area were calculated using nonlocal density functional theory (NLDFT-cylindrical model). The pore size distributions were calculated from the adsorption isotherms by nonlocal density functional theory (NLDFT).

Adsorption performance

CO_2 adsorption isotherms were measured at 273 and 298 K with a Quadrasorb SI analyser. Before the measurements, the samples were degassed in vacuum at 373 K for 12 h.

Cr (VI) ion adsorption experiments were conducted using the batch equilibration technique. In a 100 ml container, 10 mg of the MRT samples were suspended in 50 ml $K_2Cr_2O_7$ solutions with concentrations ranging from 5 to 100 mg/L. The PH was fixed at 3 by 0.1 mol/L HCl. The mixture was

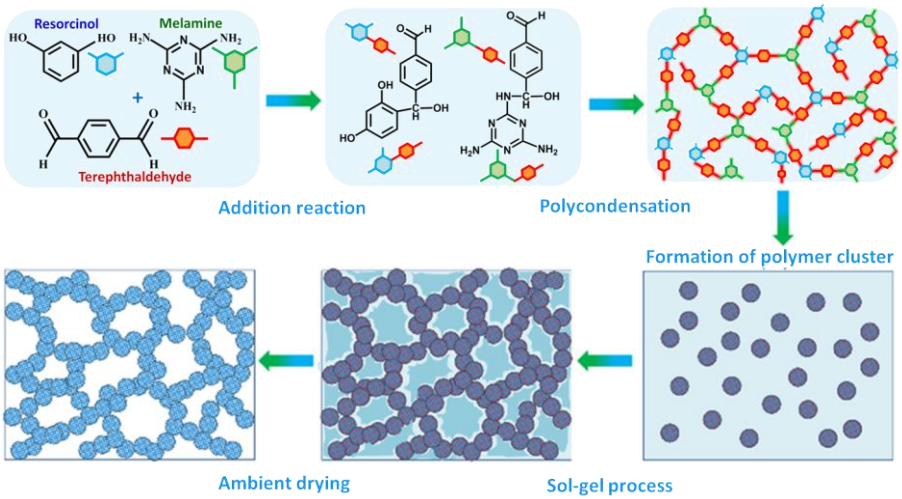

Scheme 1. The schematic illustration of the preparation of the MRT networks. The micropres are within the networks of highly cross-linked polymer clusters, while the mesopores result from a 3D continuous polymeric gel network

continuously shaken in a shaking bath at 25 °C for 24h. Then the mixture was filtered with filter paper and the residual Cr(VI) ion concentration in the filtrate was analysed by UV-vis spectrometer (UV-3150), using 1,5-diphenylcarbonohydrazide (DPC) as a chromogenic reagent.[36]

The adsorption capacities q (mg/g) was calculated by the following formulas:

$$q_t = \frac{(C_t - C_0)\times V}{m}$$

In the formula C_t and C_0 (mg/L) denote, respectively, the initial and t moment concentration of Cr(VI) in the solution. V (L) and m (g) denote the volume of Cr(VI) solution and the mass of adsorbent, respectively.

Results and discussion

Characterization of the MRT networks

Phenolic resins and melamine resins are well-known synthetic polymers made from a step-growth polymerization of phenol or melamine with formaldehyde.[37, 38] Both the resins are composed of high crosslinking 3-dimension networks, but the polymer chains, especially for methylene and methyl ether bridges are not enough rigid to prevent pack space efficiently. Inspired by their synthetic chemistry, here we used terephthaldehyde instead of formaldehyde to crosslink the resorcinol and melamine under solvothermal conditions. We hope the aromatic aldehyde could provide certain rigidity within the networks to prevent rotational freedom along the polymer backbone. The typical synthesis process for the MRT networks is illustrated in Scheme 1. According to the phenolic/melamine resin chemistry, the carbonyl group from terephthaldehyde could be attacked by the electron-rich phenyl rings or amino-group, forming the hydroxyl-containing derivatives. The polycondensation will occur among these addition derivatives under elevated temperature without using any catalysts, which can crosslink each other to form small clusters consisting of branched polymeric species. The clusters can continuously grow via further condensing to form colloid-like polymer particles. As initial particle nucleation and growth proceeds, the increasing molecular weight and branching of polymers decrease compatibility of polymer particles with solvent. Therefore, microphase separation was induced by covalent cross-linking in various directions, forming 3-D gels which span the entire volume of a fluid medium. Due to structural rigidity of the MRT networks, their micropores within the networks and mesopores among particulate network units can be retained by directly dried at the ambient conditions. It is important to note here that the micropores are logically related to the chemical cross-linked structure while the mesopores depend on the size of particulate network units themselves and their compact/loose cross-linked aggregation.

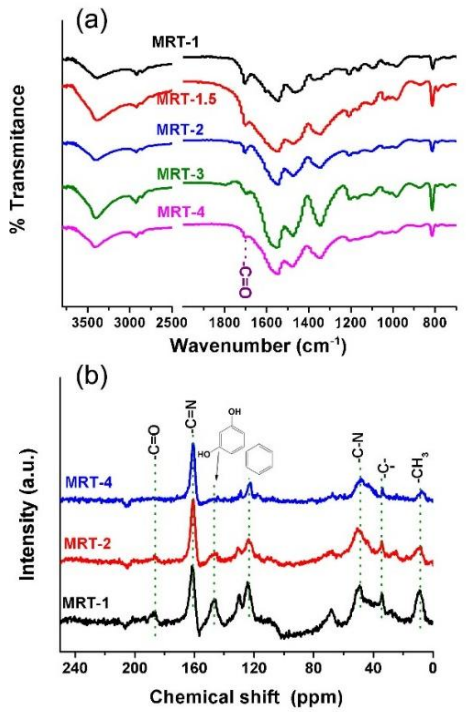

Fig. 1 The FTIR (a) and 13C solid NMR spectra of the MRT networks

The elemental compositions of the obtained MRT networks were listed in Table 1 from the CHN analysis. All samples contain a large amount of nitrogen atoms, and the nitrogen fraction follows the same trend with the calculated amount of nitrogen used in the reaction. The FTIR spectra of these samples (Figure 1a) are very similar regardless of their elemental composition. The triazine rings from melamine were inherited into the MRT networks, as indicated by two strong adsorption bands at 1508 and 1363 cm^{-1} which represent the

aromatic C–N stretching and "breathing" modes, respectively[33]. In addition, the FTIR signals corresponding to -OH groups (3300 cm-1) from resorcinol or the end functional -C-OH or the residual ethanol are also observed for all samples. The carbonyl function of the aldehydes at 1690 cm^{-1} (C=O stretching) are still observed in all samples, suggesting the aldehydes have not been completely reacted. However, it is clear the intensity of carbonyl peak decrease with the M/R ratio increasing. This result suggests the increase of melamine content could improve the polycondensation degree.

Table 1 Pore parameters and chemical nature of the MRT networks

	Chemical composition				Porosity					
Samples	C[a]	H[b]	N[c]	N[d]	S_{BET}[e]	S_{mic}[f]	V_{total}[g]	V_{mic}[h]	V_{mes}[i]	D_{BJH}[j]
	wt%	wt%	wt%	wt%	m^2/g	m^2/g	cm^3/g	cm^3/g	cm^3/g	nm
MRT-1	56.6	4.8	18.2	21.9	485	198	0.23	0.102	0.127	3.2
MRT-1.5	52.6	4.6	25	26	628	335	1.03	0.195	0.833	14
MRT-2	51.3	4.7	27.5	28.8	642	341	1.13	0.201	0.926	20
MRT-3	47.9	4.7	32.4	32.2	680	522	0.77	0.244	0.517	22
MRT-4	45.2	4.7	34.5	34.3	561	463	0.6	0.211	0.378	30

[a] Carbon content from CHN analysis; [b] Hydrogen content from CHN analysis; [c] Nitrogen content from CHN analysis; [d] Theoretical nitrogen content in the polymer; [e] BET specific surface area from N_2 adsorption; [f] DFT micropore surface area (< 2 nm); [g] total pore volume (P/P_0= 0.985); [h] DFT micropore volume (< 2 nm); [i] BJH mesopore volume; [j] BJH average pore diameter.

The MRT networks were further characterized by 13C CP-MAS NMR spectroscopy, as shown in Figure 1b. Four obvious resonances at 165, 128, 53 and 12 ppm can be observed for all samples. The first can be assigned to the carbon atoms present in the triazine ring of the melamine,[39] whereas the signal at 128-133 ppm originates from the aromatic carbons of the resorcinol and terephthaldehyde. The resonance at 50 ppm can be correlated to the tertiary carbon atoms formed upon the addition of the primary amine groups of melamine to the newly formed C-N bond.[33] The resonance at 37 ppm is assigned to the tertiary carbon formed by the condensation reaction.[28] The resonance at 12 ppm is assigned to primary CH_3 from adsorbed solvent ethanol. The peak at 150 ppm corresponds to phenoxy carbons from the resorcinol, which gradually weakens with the increase of the M/R ratio. The signal at 193 ppm is attributed to unreacted aldehydes, and its intensity gradually decreases with the increase of melamine content in precursor, in accordance with the result from the FTIR analysis. These results further confirm the increase of hexafunctional melamine content could decrease the unreacted aldehyde groups, thus improving the condensation degree of the MRT networks.

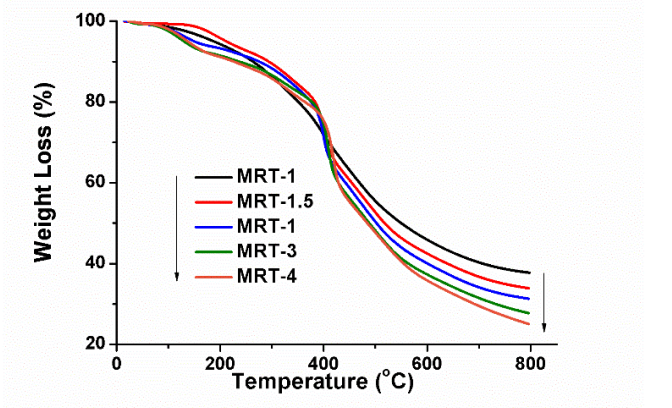

Fig. 2 Thermogravimetric analysis of the MRT networks under N_2 flow

The thermal stability of the MRT networks was investigated by thermogravimetric analysis (TGA) (Figure 2) in N_2 atmosphere. The initial weight loss up to 150 °C can be attributed to the trapped solvent in the porous network. About 10% weight loss is observed in the range of 150-350 °C and maximum weight loss occurs at temperatures of 350-600 °C due to the transformation or carbonization of the polymer framework. The carbonization yield at 800 °C is in the range of 25-47%, and it obviously decreases with the increase of M/R ratio. This is due to the melamine derivatives can be prone to pyrolysis compared to phenolic derivatives.

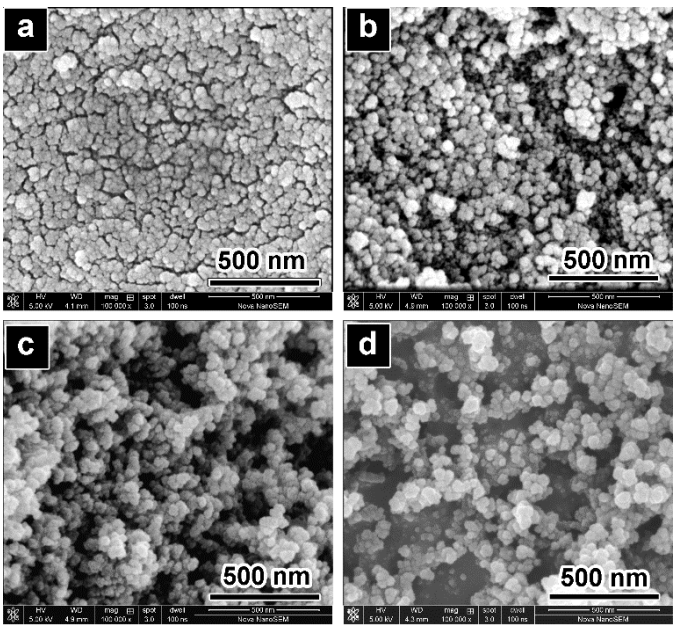

Fig. 3 SEM images of the MRT networks. (a) MRT-1, (b) MRT-2, (c) MRT-3 and (d) MRT-4

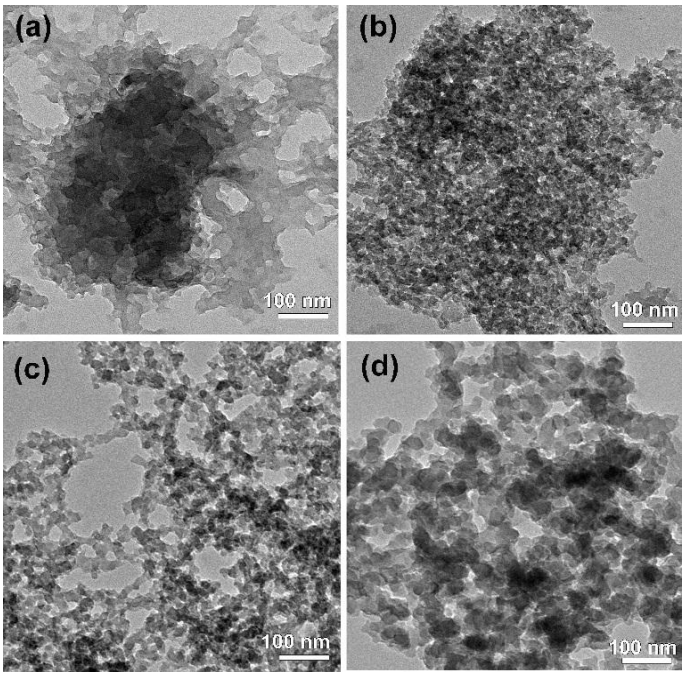

Fig. 4 TEM images of the MRT networks. (a) MRT-1, (b) MRT-1.5, (c) MRT-2 and (d) MRT-4

After having characterized the molecular structure, we investigated the morphology of the MRT networks by SEM and TEM observations. As shown in Figure 3, SEM images of the samples showed typically 3-D porous networks formed by the inter-linking of irregular particles. Interestingly, the size of the particles gradually increases with the increase of M/R ratio. And thus the resulting inter-particle pore seems to be larger gradually. TEM observations further give clear mesoporous morphology of the MRT network, as shown in Figure 4. The MRT-1 show dense packing arrangement of polymer chains, in agreement with the compact structure in SEM image. Increase the M/R ratio to 1.5, the mesopores can be easily found as void-type pores resulting from overlapping and interconnecting colloid-like polymer particles. Moreover, the particle size obviously increases with the M/R ratio, and thus the interparticulate porosity grow larger even into macroporous range (> 50 nm). In sol-gel chemistry, the initial colloid particles depend on two steps: nucleation and growth.[40] Small particles are generally obtained if the nucleation rate is very fast while the amount of materials available for growth keeps similar. Our results suggest that the high M/R ratio could slow nucleation rates and increase the time of growth stage, as a result, leading to the formation of relatively large colloid-like particles. Thus, the increase of melamine content in the networks could increase the size of particulate network units themselves, which ensure the appropriate rigidity of the network structure to avoid the collapse of internetwork pores during drying. This promises the ability to control the mesoporous structure by a rational design of the precursor composition.

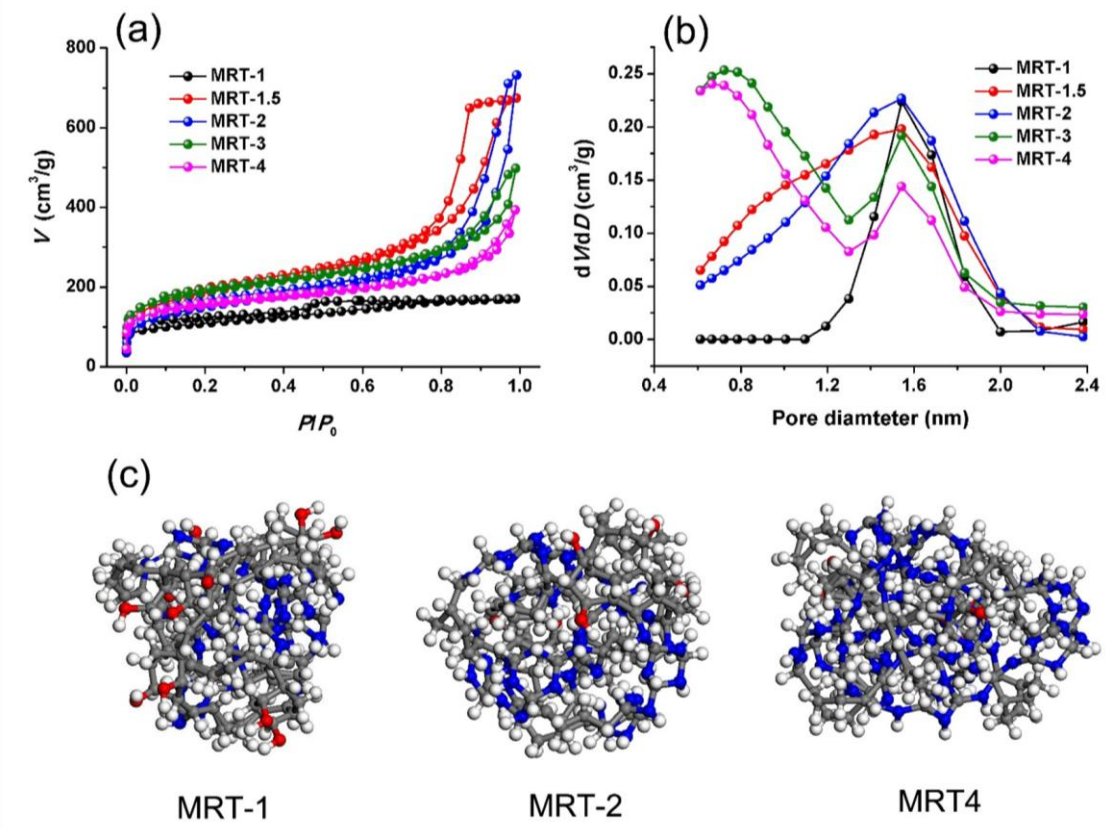

Fig. 5 N_2 adsorption isotherms (a) and the NL-DFT pore size distributions of the MRT networks. (c) The structural model of the MRT networks.

The detailed porous structure of the MRT networks was analysed using N_2 adsorption-desorption isotherms at 77 K, as shown in Figure 5. All isotherms of the MRT networks exhibit a type IV with an associated H2 hysteresis loop according to

IUPAC classification, which are attributable to capillary condensation occurring in mesopores. It is clear that the hysteresis loop gradually shift to the high relative pressure with the increase of the M/R ratio, indicating a growth of the mesopore. In addition, the high uptake of N_2 adsorption at low relative pressures in all adsorption isotherms indicates that considerable micropores exist in the polymer networks. The calculated porosity values are listed in Table 1. These samples have a BET surface area of ca. 500-600 m^2/g and an intrinsic micropore surface area of ca. 300 m^2/g. The average mesopore size generally increases with the M/R ratio, but the total pore volume and mesopore volume exhibit a maximum at the M/R of 2. Further increase the M/R ratio should extend the pore into macroporous range that cannot be effectively detected by the N_2 adsorption. This can be confirmed by SEM and TEM observations that the interconnected macropores present in the MRT-3 and MRT-4.

Except the mesoporous structure, turning M/R ratio could also lead to the change of the spatial structure of the polymer networks, and the resulting microporous structure. This can be well verified by the plots of the NL-DFT pore size distributions in Figure 5b. At the relatively low M/R ratio, the MRT-1 networks show a narrow unimodal peak centered at 1.5 nm. The increase of the M/R ratio gradually broadens this peak into smaller micropore region and even introduces a new peak located at 0.8 nm for the MRT networks. The increase of melamine content could also introduce more accessible micropores into the networks. As listed in Table 1, higher micropore surface area and larger micropore volume (< 2 nm) are obtained for the MRT networks with higher M/R ratio.

Undoubtedly, the microporosity of the MRT networks should arise simply from the covalent 3-D cross-linked network. The model presented in Fig. 5c is a schematic of the frameworks, based on the energy minimized conformations of the first generation oligomers with different M/R ratios. Obviously, the addition of hexafunctional melamine into trifunctional RT system should increase chain branching and crosslink density of polymer network, which may prohibit spatially efficient packing in the solid state. The weaken IR and NMR peaks of unreacted aldehyde groups could also demonstrate the improved condensation degree for the MRT networks with higher M/R ratio. Thus, higher corss-linking of polymer chain creates more ultra-microporosity inside the MRT network. However, compared to the phlorglucinol-terephthalaldehyde networks prepared by Kanatzidis,[41] the microporous surface area of the MRT networks prepared here is not high. Considering the structure of networks is strongly influenced from the parameters that affect the bending and twisting of polymer chains as temperature, solvent, concentration of reactants, washing and drying conditions, we hope that we can optimize the conditions to improve microporosity in the future researches.

The CO_2 adsorption

Nitrogen-rich porous polymer with a hierarchical mesoporous/microporous structure may interact attractively with acid CO_2 molecules through fast kinetic diffusion and improved molecular interaction. Herein the CO_2 uptakes of the networks were measured up to 1 bar at 273 and 298 K, as shown in Figure 6. The adsorption isotherms at 273 K have a steep rise at low pressure and slowly reach the maximum at 1 bar, and the isotherms at 298 K show a more linear CO_2 isotherms in this pressure range. Regardless of the microporsity (surface area and micropore volume), the CO_2 adsorption capacity gradually increases with the M/R ratio, and exhibit capacity of 2.3 mmol/g at 273 K and 2.1 mmol/g at 298 K for MRT-4. Compared to other microporous organic polymers with high surface area (> 1000 m^2/g), the MRT networks prepared in this work have been uncompetitive in the surface area, however, their CO_2 uptakes at 1 bar and 298 K are really impressive, where the published values of microporous organic polymers are generally less than 2.0 mmol/g in this pressure-temperature regime.[42-48]

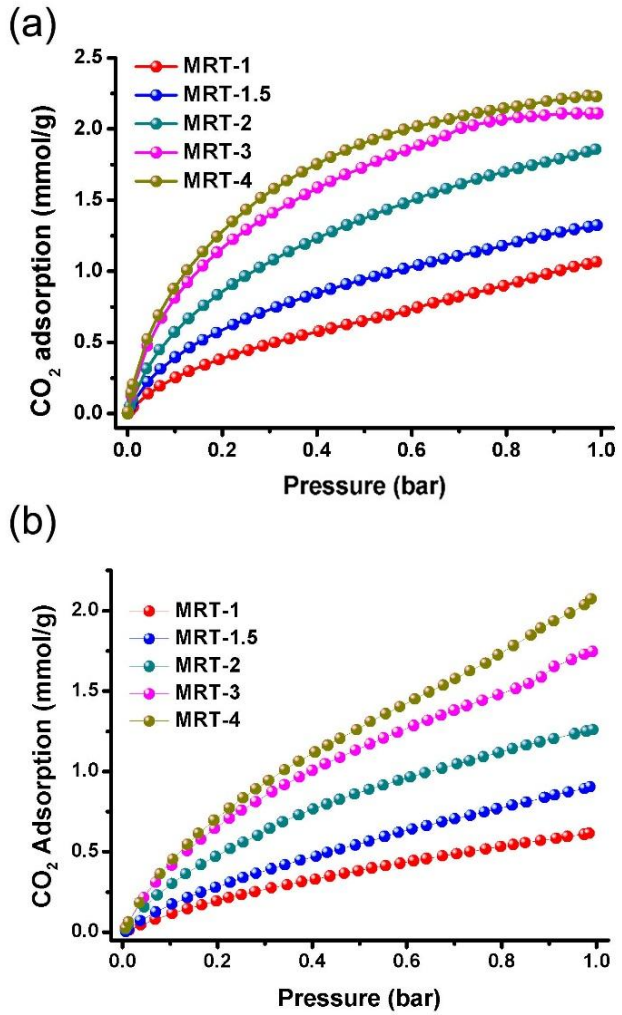

Fig. 6 CO_2 adsorption isotherms of the MRT networks at 273 K (a) and 298 K (b)

It is clear from the data in Table 1 that the apparent BET surface area, as measured by N_2 adsorption, has little relationship to the amount of CO_2 adsorbed at 1 bar. This can be further confirmed that, despite the very high BET surface areas of some microporous organic polymers, the resulting CO_2 uptakes are lower than many materials with much lower surface areas.[43] Thus, the uptake of CO_2 should be more related to the pore size in the networks, with the smallest pores contributing most to the uptake of CO_2 at low pressures. The plot shown in Figure 5b shows quite clearly that the high M/R ratio could introduce more ultra-micropores. Previous reports also revealed that micropores less than 1.2 nm would be effective towards CO_2 capture.[48] The smaller micopore size and higher ultra-micropores surface area should be one of reasons for higher CO_2 capacity of the MRT networks with higher M/R ratio. On the other hand, the polarizability and large quadrupole moment (4.3×10^{-26} esu cm^2) of CO_2 can be taken advantage of by

introducing functional groups that create strong interactions between the material surface and CO_2. To determine the strength of the interaction between CO_2 molecular and the MRT networks, the isosteric heat (Q_{st}) of CO_2 adsorption (shown in Figure S1) is calculated using CO_2 adsorption isotherms at 273 and 298 K based on the Clausius-Clapeyron equation.[34] It can be found that the MRT networks with higher M/R ratio have higher isosteric heat at low coverage. This means the MRT-4 possesses more high-energy sites for CO_2 adsorption which are preferentially occupied by CO_2. We suspect that the presence of amine functional groups from melamine precursor, is the source of its energetic heterogeneity for CO_2 adsorption. The synergistic effects of ultramicroporosity and enhanced molecular interaction therefore improve the CO_2 adsorption capacity for the MRT-3 and MRT-4.

The Cr(VI) ion adsorption performance

The MRT networks are internally decorated with a large number of functional groups such as –NH from melamine and –OH from resorcinol, which may serve as irregular sites with chemical heterogeneity available for metal ion adsorption. As a proof-of-concept application, we studied their adsorption ability towards Cr (VI) ions, which is one of typical heavy metal ions in industrial wastewater. Fig. 7 shows Cr (VI) ion adsorption isotherms at 25 ^{o}C at pH 3. All the isotherms show a steep initial slope indicating high efficiency of the material at low concentration. The MRT-1 exhibits the minimum adsorption capacity, possibly due to the relatively low surface area and small mesopore size that limits the intraparticle diffusion. The MRT-1.5 has a maximum uptake of 126.3 mg/g. However, the other samples show a decrease in Cr (VI) uptakes with the increase of the M/P ratio, even though their micropore surface area and micrpore volume gradually increase. This result suggests that the other factor rather than microporosity should play a dominate role on the Cr (VI) ion adsorption.

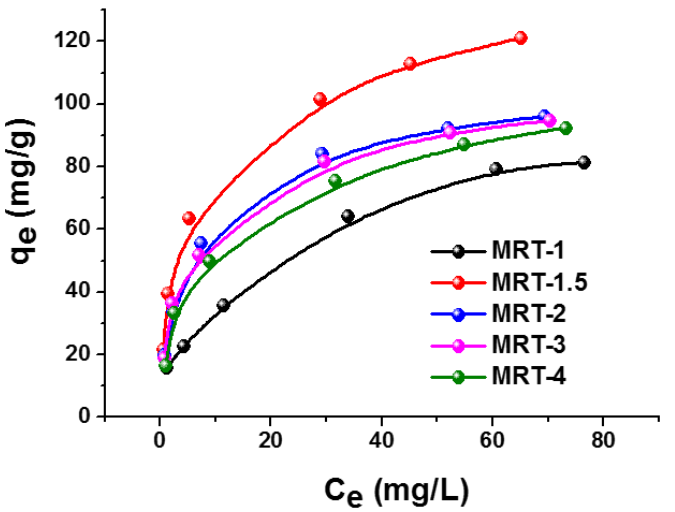

Fig. 7 Adsorption isotherms for Cr(VI) on the MRTs

To further understand the mechanism of the adsorption, the equilibrium adsorption isotherms are analyzed using Langmuir and Freundlich modes (Figure S2, Figure S3). The Langmuir adsorption isotherm assumes that the adsorption can only occur at a fixed number of definite localized sites, each site can hold only one adsorbate molecule (monolayer), and the sites are homogeneous. And there is no interaction between adsorbed molecules and the surface of the heterogeneous catalytic reactions.[49] The Freundlich isotherm is mostly used to describe the nonideal sorption that involves heterogeneous sorption.[50] The obtained parameters for the two models are listed in Table S1. The data fit well with both isotherm models, but give a better fit to the Freundlich model. This result suggests the heterogeneous surface adsorption should also contribute to the Cr (VI) ions removal, responding to the typical ion exchange behaviour. Furthermore, the value of Freundlich constant n, which is dimensionless and represents adsorption intensity, decreases gradually with the increase of M/R ratio. This result indicates the MRT networks with lower M/R ratio have higher energetic heterogeneity of the adsorption sites. Looking inside the chemical composition of the MRT networks, the end-cap functional groups majorly include the –OH groups from the resorcinol and the –NH groups from melamine. The former decreases while the latter increases with the increase of the M/R ratio. Therefore, it is reasonably conclude that the OH groups should be the heterogeneous sites for the Cr (VI) ion adsorption.

Conclusions

In a conclusion, we demonstrated a facile method to prepare the hierarchical nitrogen-rich porous polymer, which combining the micropores formed from a network of rigid polymer chains with the meso-/macropores formed from the reaction-induced sol-gel phase separation. The polycondensation of melamine, resorcinol and terephthaldehyde could form rigid polymer chains in molecular level and rigid polymer clusters in mesoscopic level, thus withdrawing high capillary pressure to maintain simultaneously the micropores inside the MRT networks and mesopores between interconnected polymer particles. Moreover, the microporous structure, mesoporous structure and chemical functionalities can be easily adjusted only by changing the M/R ratio in the precursor. The obtained MRT networks have hierarchical structure with moderate surface area; however their CO_2 uptakes at 1bar and 298k are comparable to most high-surface-area microporous polymers. In addition, their rich surface functional groups could serve as irregular sites with chemical heterogeneity available for Cr (VI) ion adsorption. Because of their low-cost and facile synthesis, high thermal stability, as well as tunable hierarchical porosity and chemical composition, the presented MRT networks are emerging as new adsorbents, which may have good potential applications in the gas separation and heavy metal ion adsorption.

Acknowledgements

This work was partly supported by MOST (2014CB239702) and National Science Foundation of China (No. 51302083, No. 51172071, No.51272077), and Fundamental Research Funds for the Central Universities and Shanghai Pujiang Program.

Notes and references

[a] State Key Laboratory of Chemical Engineering, East China University of Science and Technology, Shanghai 200237, China.
[b] National Engineering Laboratory for Carbon Fiber Technology, Institute of Coal Chemistry, Chinese Academy of Sciences, Taiyuan 030001, China.
† These authors contributed equally to this work.
*Corresponding author: Donghui Long, Tel: +86 21 64252924, Fax: +86 21 64252914. E-mail: longdh@mail.ecust.edu.cn; Chunxiang Lv, E-mail: lucx@sxicc.ac.cn.

Electronic Supplementary Information (ESI) available: [More results including isosteric heat of CO_2 adsorption, equilibrium adsorption modeling for Cr (VI) adsorption]. See DOI: 10.1039/b000000x/

1 J. X. Jiang and A. I. Cooper, *Top Curr. Chem*., 2010, **293**, 1-33.
2 K. E. Maly, *J. Mater. Chem*., 2009, **19**, 1781-1787.
3 D. C. Wu, F. Xu, B. Sun, R. W. Fu, H. K. He, and K. Matyjaszewski, *Chem. Rev.*, 2012, **112**, 3959-4015.
4 P. Kaur, J. T. Hupp and S. T. Nguyen, *ACS Catal.* 2011, **1**, 819-835.
5 S. Makhseed, F. Al-Kharafi, J. Samuel and B. Ateya, *Catal. Commun.*, 2009, **10**, 1284–1287.
6 J. Schmidt, J. Weber, J. D. Epping, M. Antonietti and A. Thomas, *Adv. Mater.*, 2009, **21**, 702-705.
7 N. B. McKeown and P. M.Budd, *Chem. Soc. Rev.*, 2006, **35**, 675-683.
8 A. I. Cooper. *Adv. Mater.* 2009, **21**, 1291-1295.
9 S. S. Han, H. Furukawa, O. M. Yaghi and W. A.Goddard, *J. Am. Chem. Soc*., 2008, **130**, 11580-11581.
10 W. G. Lu, D. Q.Yuan, D. Zhao, C. I. Schilling, G. Plietzsch, T. Muller, S. Bräse, J. Guenther, J. Blümel, R. Krishna, Z. Li and H. C. Zhou, *Chem. Mater*., 2010, **22**, 5964-5972.
11 V. A. Davankov and M. P.Tsyurupa, *React. Polym.* 1990, **13**, 27-42.
12 M. G. Schwab, I. Senkovska, M. Rose, N. Klein, M. Koch, J. Pahnke, G. Jonschker, B. Schmitz, H. Michael and S. Kaskel, *Soft Matter* 2009, **5**, 1055-1059.
13 J. Germain and J. M. J. Frechet and F. Svec, *J. Mater. Chem.*, 2007, **17**, 4989-4997.
14 C. D.Wood, B.Tan, A.Trewin, H. Niu, D.Bradshaw, M. J. Rosseinsky, Y. Z. Khimyak, N. L. Campbell, R. Kirk, E. Stöckel and A. I. Cooper, *Chem. Mater*., 2007, **19**, 2034-2048.
15 H. J. Mackintosh, P. M. Budd and N. B. McKeown, *J. Mater. Chem.*, 2008, **18**, 573-578.
16 P. M. Budd, N. B. McKeown and D. Fritsch, *J. Mater. Chem.*, 2005, **15**, 1977-1986.
17 J. X. Jiang, F. Su, A. Trewin, C. D. Wood, N. L. Campbell, H. Niu, C. Dickinson, A. Y. Ganin, M. J. Rosseinsky, Y. Z. Khimyak and A. I. Cooper, *Angew. Chem. Int. Ed. Eng.* 2007. **46**, 8574-8578. see also correction, *Angew. Chem. Int. Ed. Eng.*, 2008. **47**, 1167.
18 J. X. Jiang, F. Su, A. Trewin, C. D. Wood, H. Niu, J. T. A. Jones, Y. Z. Khimyak and A. I. Cooper, *J. Am. Chem. Soc.*, 2008, **13**, 7710-7720.
19 A. P. Cote, A. I. Benin, N.W. Ockwig, M. O'Keeffe, A. J. Matzger and O. M.Yaghi, *Science*, 2005, **310**, 1166-1170.
20 H. M. El-Kaderi, J. R. Hunt, J. L. Mendoza-Cortes, A. P. Cote, R. E. Taylor, M. O'Keeffe and O. M. Yaghi, *Science* 2007, **316**, 268-272.
21 A. P. Cote, H. M. El-Kaderi, H. Furukawa, J. R. Hunt and O. M. Yaghi, *J. Am. Chem. Soc.*, 2007, **129**, 12914-12915.
22 P. M. Budd. *Science* 2007, **316**, 210-2011.
23 S. Y. Moon, J. S. Bae, E. Jeon and J. W. Park, *Angew. Chem., Int. Ed*., 2010, **49**, 9504-9508.
24 S. Y. Moon, H. R. Mo, M. K. Ahn, J. S. Bae, E. Jeon and J. W. Park, *J. Polym. Sci., Part A: Polym. Chem*., 2013, **51**, 1758-1766.
25 S. Y. Moon, E. Jeon, J. S. Bae, M. Byeon and J. W. Park, Polym. Chem., 2014, **5**, 1124–1131.
26 B. L. Su, C. Sanchez and X. Y. Yang. Hierarchically Structured Porous Materials. Wiley-VCH, Weinheim: 2011.
27 A. P. Katsoulidis and M. G. Kanatzidis, *Chem. Mater.*, 2012, **24**, 471-479.
28 A. P. Katsoulidis, J. Q. He and M. G. Kanatzidis, *Chem. Mater*., 2012, **24** , 1937-1943.
29 X. Du, Y. Sun, B. Tan, Q. Teng, X.Yao, C. Su and W. Wang, *Chem. Commun.*, 2010, **46**, 970-972.
30 Y. Zhang, S. N. Riduan and J. Y. Ying, *Chem.-Eur. J.*, 2009, **15**, 1077-1081.
31 P. X. Hou, H. Orikasa, T. Yamazaki , K. Matsuoka, A. Tomita, N. Setoyama, Y. Fukushima and T. Kyotani, *Chem. Mater.*, 2005, **17**, 5187-5193.
32 W. G. Lu, J. L. P. Sculley, D. Q.Yuan, R. Krishna, Z. W. Wei and H. C. Zhou, *Angew. Chem. Int. Ed.*, 2012, **51**, 1-6.
33 M. G. Schwab, B. Fassbender, H. W. Spiess, A. Thomas, X. L. Feng and K. Mullen, *J. Am. Chem. Soc*., 2009, **131**, 7216-7217.
34 R. Dawson, D. J. Adams and A. I. Cooper, *Chem. Sci.*, 2011, **2**, 1173-1177.
35 Y. Li, S. M. Zhu, Q. L. Liu, Z. X. Chen, J. J Gu, C. L. Zhu, T. Lu, D. and Zhang, J. Ma, *Water Research, 2013*, **47**, 4188-4197.
36 K. Parida, K. G. Mishra and S. K. Dash, *J. Hazar. Mater.*, 2012, **241**, 395-403.
37 A. Gardziella, L. A. Pilato and A. Knop Phenolic Resins Chemistry, Applications, Standarisation, Safety and Ecology, Springer-Verlag, Berlin Heidelberg, 2000.
38 P. Swaraj. Surface Coatings: Science and Technology, 2d ed. Chichester, John Wiley, 1997.
39 H. H. Zhou, S. Xu, H. P. Su, M. Wang, W. M. Qiao, L. C. Ling and D. H. Long, *Chem. Commun*., 2013, **49**, 3763-3765.
40 C. J. Brinker and G. W. Scherer. Sol-Gel Science: The physics and Chemistry of Sol-Gel Processing. Academic Press, San Diego, CA, 1990.
41 A. P. Katsoulidis and M. G Kanatzidis, *Chem. Mater.*, 2011, **23**, 1818-1824.
42 H. Furukawa and O. M. Yaghi, *J. Am. Chem. Soc*., 2009, **131**, 8875-8883.
43 R. Dawson, E. Stcockel, J. R. Holst, D. J. Adams and A. I. Cooper, *Energy Environ. Sci*., 2011, **4**, 4239-4245.
44 K. B. Lee, M. G.Beaver, H. S. Caram and S. Sircar, *Ind. Eng. Chem. Res*., 2008, **47**, 8048-8062.
45 C. F. Martin, E. Stcockel, R. Clowes, D. J. Adams, A. I. Cooper, J. J. Pis, F. Rubiera and C. Pevida, *J. Mater. Chem*., 2011, **21**, 5475-5483.
46 T. Ben, C. Pei, D. Zhang, J. Xu, F. Deng, X. Jing and S. Qiu, *Energy Environ. Sci*., 2011, **4**, 3991-3999.
47 Z. Yang, Y. Xia and R. Mokaya, *J. Am. Chem. Soc*., 2007, **129**, 1673-1679.
48 A.Wahby, J. M. Ramos-Fernandez, M. Martınez-Escandell, A. Sepuveda-Escribano, J. Silvestre-Albero and F. Rodrıguez-Reinoso, *ChemSusChem*, 2010, **3**, 974–981.
49 D. P. Das, K. M. Parida and B. R. De, *J. Mol. Catal. A: Chem*., 2006, **245**, 217-224.
50 R. Schmuhl, H. M. Krieg and K. Keizer, *Water S.A.*, 2001, **27**, 1-7.

